

Article

Characterization of Silver Carbonate Nanoparticles Biosynthesized Using Marine *Actinobacteria* and Exploring of Their Antimicrobial and Antibiofilm Activity

Omar Messaoudi ^{1,2} , Ibrahim Benamar ^{1,2} , Ahmed Azizi ³, Salim Albukhaty ^{4,5,*} , Yasmina Khane ⁶ , Ghassan M. Sulaiman ⁷ , Mounir M. Salem-Bekhit ⁸, Kaouthar Hamdi ¹, Sirine Ghoummid ¹, Abdelhalim Zoukel ^{9,10}, Ilhem Messahli ¹, Yacine Kerchich ¹¹, Farouk Benaceur ^{1,12} , Mohamed M. Salem ¹³  and Mourad Bendahou ²

- ¹ Department of Biology, Faculty of Science, University of Amar Telidji, Laghouat 03000, Algeria; o.messaoudi@lagh-univ.dz (O.M.); ib.benamar@lagh-univ.dz (I.B.); k.hamdi.bio@lagh-univ.dz (K.H.); goumidisrine@gmail.com (S.G.); messahli.ilhem@gmail.com (I.M.); f.benaceur@lagh-univ.dz (F.B.)
 - ² Laboratory of Applied Microbiology in Food and Environment, Abou Bekr Belkaid University, Tlemcen 13000, Algeria; bendahou63@yahoo.fr
 - ³ Department of The Common Trunk Sciences and Technology, Faculty of Technology, University of Amar Telidji, Highway Ghardaia, P.O. Box G37 (M'kam), Laghouat 03000, Algeria; a.azizi@lagh-univ.dz
 - ⁴ Department of Chemistry, College of Science, University of Misan, Maysan 62001, Iraq
 - ⁵ College of Medicine, University of Warith Al-Anbiyaa, Karbala 56001, Iraq
 - ⁶ Faculty of Science and Technology, University of Ghardaia, BP455, Ghardaia 47000, Algeria; yasminekhane@yahoo.fr
 - ⁷ Division of Biotechnology, Department of Applied Sciences, University of Technology, Baghdad 10066, Iraq; ghassan.m.sulaiman@uotechnology.edu.iq
 - ⁸ Department of Pharmaceutics, College of Pharmacy, King Saud University, P.O. Box 2457, Riyadh 11451, Saudi Arabia; mbekhet@ksu.edu.sa
 - ⁹ Laboratory Physico-Chemistry of Materials, Laghouat University, Laghouat 03000, Algeria; abdelhalim.zoukel@gmail.com
 - ¹⁰ Center for Scientific and Technical Research in Physicochemical Analysis (PTAPC-Laghouat-CRAPC), Laghouat 03000, Algeria
 - ¹¹ École Nationale Polytechnique (ENP), Laboratory of Environmental Science and Technology, El Harrach 16200, Algeria; yacine.kerchich@g.enp.edu.dz
 - ¹² Research Unit of Medicinal Plant (RUMP) Attached to Center of Biotechnology (CRBt, 3000, Constantine), Laghouat 03000, Algeria
 - ¹³ College of Medicine, Huazhong University of Science and Technology, Wuhan 430030, China; medozcockney@gmail.com
- * Correspondence: albukhaty.salim@uomisan.edu.iq



Citation: Messaoudi, O.; Benamar, I.; Azizi, A.; Albukhaty, S.; Khane, Y.; Sulaiman, G.M.; Salem-Bekhit, M.M.; Hamdi, K.; Ghoummid, S.; Zoukel, A.; et al. Characterization of Silver Carbonate Nanoparticles Biosynthesized Using Marine *Actinobacteria* and Exploring of Their Antimicrobial and Antibiofilm Activity. *Mar. Drugs* **2023**, *21*, 536. <https://doi.org/10.3390/md21100536>

Academic Editors: María Carmen Rodríguez-Argüelles and Noelia González-Ballesteros

Received: 20 September 2023
Revised: 10 October 2023
Accepted: 11 October 2023
Published: 13 October 2023



Copyright: © 2023 by the authors. Licensee MDPI, Basel, Switzerland. This article is an open access article distributed under the terms and conditions of the Creative Commons Attribution (CC BY) license (<https://creativecommons.org/licenses/by/4.0/>).

Abstract: Bacterial resistance to different antimicrobial agents is growing with alarming speed, especially when bacterial cells are living in biofilm. Hybrid nanoparticles, synthesized through the green method, hold promise as a potential solution to this challenge. In this study, 66 actinomycete strains were isolated from three distinct marine sources: marine sediment, the algae *Codium bursa*, and the marine sponge *Chondrosia reniformis*. From the entirety of the isolated strains, one strain, S26, identified as *Saccharopolyspora erythrea*, was selected based on its taxonomic position and significant antimicrobial activity. Using the biomass of the selected marine *Actinobacteria*, the green synthesis of eco-friendly silver carbonate nanoparticles (BioAg₂CO₃NPs) is reported for the first time in this pioneering study. The BioAg₂CO₃NPs were characterized using different spectroscopic and microscopic analyses; the synthesized BioAg₂CO₃NPs primarily exhibit a triangular shape, with an approximate size of 100 nm. Biological activity evaluation indicated that the BioAg₂CO₃NPs exhibited good antimicrobial activity against all tested microorganisms and were able to remove 58% of the biofilm formed by the *Klebsiella pneumoniae* kp6 strain.

Keywords: isolation; marine *Actinobacteria*; *Saccharopolyspora erythrea*; silver carbonate nanoparticles; antimicrobial; antibiofilm

1. Introduction

Bacterial resistance to different antimicrobial agents, such as antibiotics, disinfectants, antiseptics, and food preservatives, arises when microbial cells become no longer sensitive to the antimicrobial agents at the concentrations used in practice. This resistance has significant health, economic, and environmental implications [1]. Compared to planktonic cells, various studies have demonstrated that bacterial resistance increases significantly when cells are in the biofilm state. Biofilm represents a unique microbial lifestyle, where bacteria are attached to a solid surface and enclosed within a self-produced extracellular polymeric substance, primarily composed of exopolysaccharides and proteins [2,3]. Consequently, both natural and synthetic classes of antimicrobial agents are currently unable to evade this phenomenon [4]. The current progress in addressing both bacterial resistance and biofilm problems involves the application of metallic nanoparticles obtained from green synthesis. This cutting-edge solution, derived from nanobiotechnology, is considered a boon in both the medical and industrial domains [5–7]. Different metals have been used for nanoparticle biosynthesis; however, the recent trend in this field is the biosynthesis of hybrid nanoparticles, combining multiple metal or mineral components to form novel nanomaterials. This approach allows for the enhancement of their properties, offering promising potential to effectively combat microbial resistance and tackle biofilm-related issues. Different biological entities can be used for the biosynthesis of nanoparticles, such as plants, fungi, and bacteria. Among bacteria, actinomycetes are well known for being a promising source of bioactive metabolites, making them particularly suitable for the synthesis of eco-friendly, cost-effective, and non-toxic metallic nanoparticles [8–11].

These filamentous bacteria are widely distributed and can be isolated from various terrestrial and marine environments. One of the well-known marine environments recognized for its geo-biodiversity is the Mediterranean coastline, which hosts more than 7% of the world's marine biodiversity, encompassing marine sediments, sponges, and algae, all of which are notable for their richness in actinomycete strains [12–14]. This coastal expanse holds the Algerian coast which spans 1622 km, and represents a yet untapped ecosystem, teeming a potential diversity of *Actinobacteria* strains, waiting to be discovered and harnessed [15–17]. Therefore, in response to the lack of published research material on such an important topic, this study sought to gather data on: (i) isolation, molecular identification, and assessment of the antimicrobial activity of marine actinomycetes isolated from sediments, algae, and marine sponges collected from the west coast of Algeria; (ii) the green synthesis of silver carbonate nanoparticles using marine *Actinobacteria* strain, followed by their characterization with a range of microscopic and spectroscopic techniques; and (iii) assessment of the biological activity of the biosynthesized silver carbonate nanoparticles.

2. Results and Discussion

2.1. Actinomycetes Isolation

In this study, we attempted to investigate the biodiversity of actinomycetes strains isolated from Algerian marine environments, such as sponges, algae, and marine sediment. The obtained results are summarized in Figure 1.

A total of 66 *Actinobacteria* strains were isolated from different marine sources collected from two sites along the Algerian coast, using four different culture media. The obtained *Actinobacteria* strains (66 isolates) were distributed based on their marine origins as follows: 46 strains were from marine sediment (70%), 15 isolates from the marine algae *Codium bursa* (23%), and 5 strains from the marine sponge *Chondrosia reniformis* (7%) (Figure 1A).

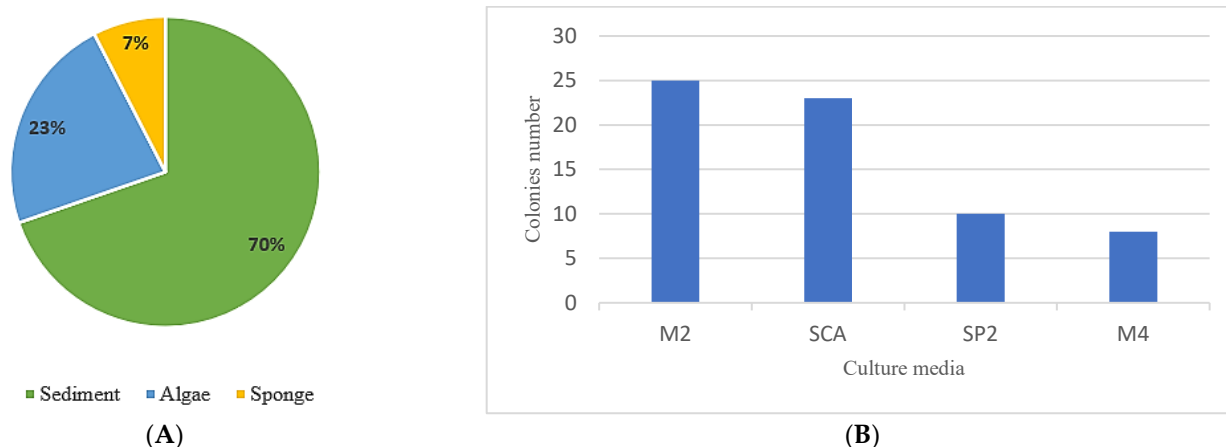


Figure 1. Distribution of the 66 *Actinobacteria* strains, according to (A) the percentage of actinomycete isolated from each marine source used, and (B) the number of actinomycete strain colonies obtained from each selective culture media used.

The selection of the two marine organisms, *Codium bursa* and *Chondrosia reniformis*, for actinomycete isolation in the current study was motivated by the absence of previous research on the diversity of *Actinobacteria* linked to these marine sources collected from the Mediterranean coast.

Previous studies have reported that sponges and algae host substantial microbial biomass, encompassing archaea, fungi, viruses, and bacteria. This symbiotic interaction yields diverse beneficial outcomes for both entities, including nutrient acquisition, metabolic processing, and chemical defense [18–20]. Moreover, several reports highlighted that marine sediments offer an excellent opportunity for the discovery of new microorganisms, which may contain a new gene cluster for the biosynthesis of novel natural products [21–23].

Furthermore, the Algerian coastal region stretches for 1622 km. Despite this long distance, this environment remains poorly investigated in terms of the biodiversity of microorganisms, including *Actinobacteria*, as an attractive source of new bioactive compounds, and only a few studies have been reported. Djinni et al., 2014 [24] isolated the marine strain *Streptomyces sundarbansensis* from brown algae collected from the Algerian coastline. This strain produces the [=2-hydroxy-5-((6-hydroxy-4-oxo-4H-pyran-2-yl)methyl)-2-propylchroman-4-one] compound, which exhibits activity against Methicillin-resistant *Staphylococcus aureus* (MRSA). In another study, Ouchene et al., 2021 [25] obtained numerous *Actinobacteria* strains from the coast of Bejaia City (Algeria), using different selective isolation methods.

Moreover, previous studies showed that the composition of culture media significantly affected the number and diversity of *Actinobacteria* strains [26–28]. Therefore, to enhance the isolation of *Actinobacteria* from the three marine sources, four culture media were used. The results indicated that SCA and M2 were the most efficient culture media for actinomycete isolation since 25 and 23 actinomycete strains were obtained from each culture medium, respectively. However, ISP₂ and M4 provide only 10 and 8 *Actinobacteria* strains, respectively (Figure 1B).

2.2. Antimicrobial Activity of *Actinobacteria* Strains

Actinobacteria isolates were evaluated for their antibacterial activity against a panel of three Gram-negative bacteria and four Gram-positive bacteria, in addition to one yeast. The results are given in Supplementary Table S1. The results revealed that 40 strains out of 66 obtained isolates, showed antimicrobial activity at least against one of the tested microorganisms. From the active strains, 30 isolates were obtained from the marine sediment, while 7 strains were isolated from the marine algae *Codium bursa*, whereas three active strains were isolated from the marine sponge *Chondrosia reniformis*. Furthermore, 26 strains exhib-

ited antifungal activity against the yeast *C. albicans*, while 29 strains were active against Gram-positive bacteria and 3 strains showed activity against Gram-negative bacteria; however, 4 strains exhibited activity against both Gram-positive and Gram-negative bacteria. Therefore, the *Actinobacteria* strains showed higher activity against Gram-positive bacteria than Gram-negative bacteria. This difference in sensitivity can be ascribed to the morphological difference between the cell walls of Gram-positive and Gram-negative bacteria, in particular, the presence of lipopolysaccharides in the outer membrane of Gram-negative bacteria, which makes the bacterial cell more impermeable to the lipophilic compounds. However, Gram-positive bacteria are more susceptible due to the absence of lipopolysaccharides [29]. Regarding resistance, *L. monocytogenes* was the most resistant bacteria tested. This resistance can be attributed to intrinsic mechanisms, such as efflux pumps, which can pump out or neutralize antimicrobial compounds, making the eradication of *L. monocytogenes* challenging [1]. In contrast, *Bacillus cereus* and *Micrococcus lotus* were the most sensitive tested microorganisms. The highest inhibition area values ranged from 21 to 30 mm, and they were observed for strain S26 against the four tested bacteria: *A. baumannii*, *S. aureus*, *M. luteus*, and *B. cereus*.

2.3. Biodiversity of Marine Actinobacteria

Partial 16S rRNA gene sequencing was used to identify 19 *Actinobacteria* strains that exhibit the highest antimicrobial activity against the tested microorganisms. By using BLAST analysis, the obtained sequences were compared to the closest homologous sequences. The results of molecular identification, shown in Supplementary Table S2, indicated that the identified isolates shared sequence similarities that ranged from 99 to 100% with 3 different *Actinobacteria* genera, including *Streptomyces* (11 strains), *Nocardiopsis* (7 strains), and *Saccharopolyspora* (1 strain). Previous studies indicated that the genera *Streptomyces*, *Nocardiopsis*, and *Saccharopolyspora* have been widely isolated from different marine sources, which were collected from distinct geographical locations, including marine sediments [30], marine sponges [31,32], marine invertebrates such as corals [33] and molluscs [34], and algae [16]. After the molecular identification of the 19 active strains, 9 actinobacterial isolates, which exhibited the best antimicrobial activity against the pathogenic microorganisms, were selected for phylogenetic study. This aimed to determine the phylogenetic relationships between the selected strains and the closest species. The results are shown in Figure 2. The obtained dendrogram differentiated the nine selected strains into three clusters. In fact, the strains V17, CS44, RH94, and S29, were spread in four different phyletic lines within the *Streptomyces* group, and they showed 99.50%, 99.30%, 99.75%, and 99.75% of sequence similarity, with type strains, *Streptomyces sampsonii* DSM 40394, *Streptomyces pseudogriseolus* strain NRRL B-3288, *Streptomyces fulvissimus* strain DSM 40593, and *Streptomyces armeniacus* DSM 43125, respectively. However, the isolates C19, CHB2, A58, and M23, which belong to the *Nocardiopsis* cluster (Figure 2), form three separated branches within the phylogenetic tree and are close to the species *Nocardiopsis terrae* YIM 90022 (99.30% similarity), *Nocardiopsis arvandica* DSM 45278 (100% similarity), and *Nocardiopsis dassonvillei* IMRU 509 (99.75% similarity), respectively. Strain S26 forms a separate clade, and it is close to the species *Saccharopolyspora erythraea*, with 99.70% similarity.

Considering the results of molecular identification coupled with antimicrobial activity, the strain S26 was selected for the preparation of silver carbonate nanoparticles ($\text{Ag}_2\text{CO}_3\text{NPs}$). This was because it belongs to a rare *Actinobacteria* genus, *Saccharopolyspora*, and because it was the most active isolate from the strains recovered from the marine Algerian environment (Supplementary Table S1).

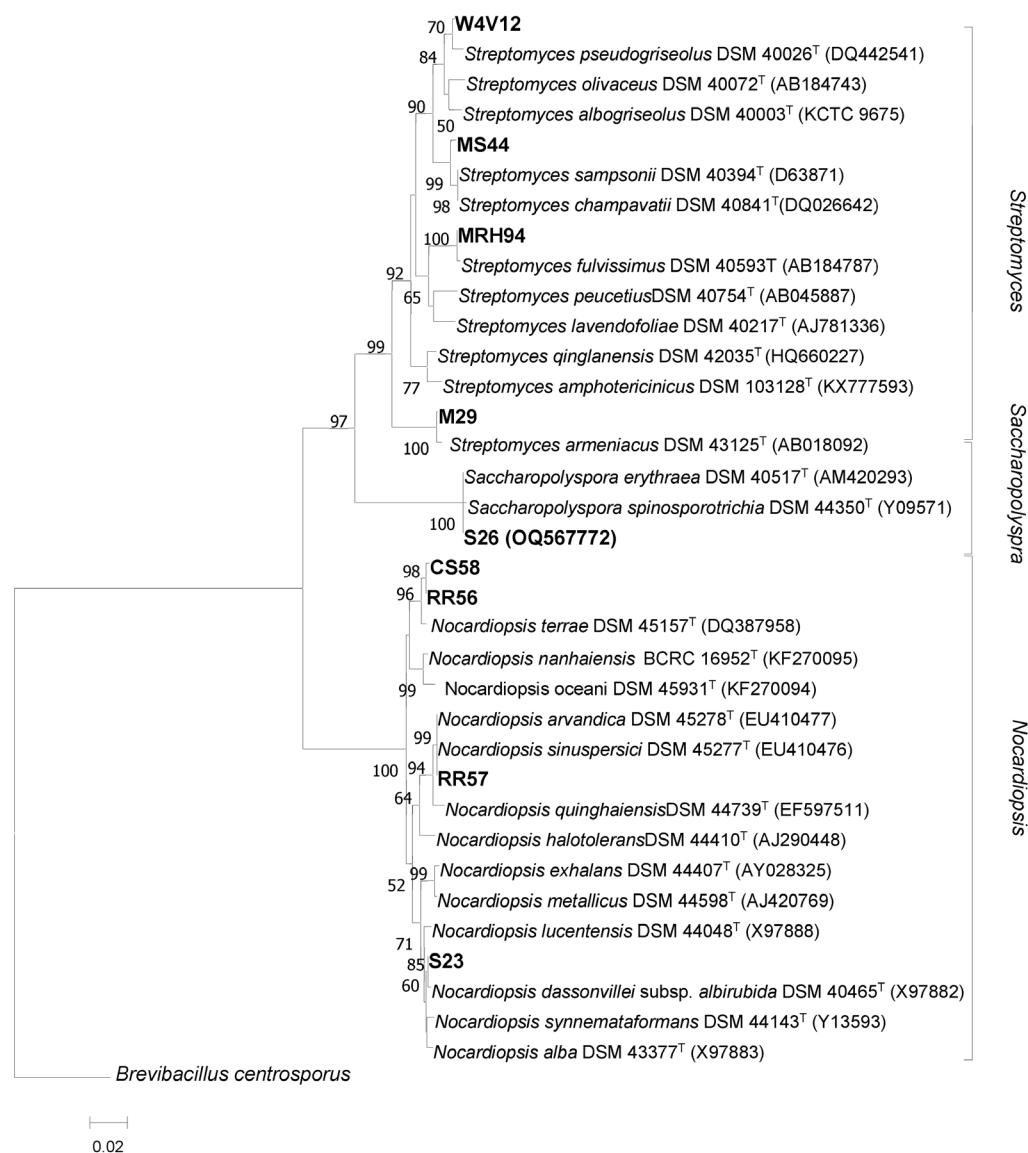


Figure 2. Neighbor-joining phylogenetic tree based on partial 16S rRNA gene sequencing, showing the phylogenetic relationship between the nine selected strains and the type strains of the closest species. Numbers at the nodes are bootstrap values, expressed as a percentage of 1000 resamplings (only values 50% are shown).

2.4. Identification of the Selected Strain S26

The selected strain S26 was identified as belonging to the genus *Saccharopolyspora*, which includes 46 species with validly published names (LPSN: <https://www.bacterio.net>, accessed on 12 October 2023). The genus *Saccharopolyspora* is a member of the family *Pseudonocardiaceae*, order *Actinomycetales*, and phylum *Actinobacteria*. Molecular identification indicated that this strain was close to the species *Saccharopolyspora erythraea* DSM 40517^T. Strains of this species are characterized by the formation of long spore chains that are surrounded by a spiny surface sheath. However, the other species belong to the *Saccharopolyspora* genus and form a smooth surface sheath [35]. Therefore, in order to verify whether the micromorphology of strain S26 is identical to the type strain *Saccharopolyspora erythraea* DSM 40517^T or not, scanning electronic microscopy was performed. The results (Figure 3) indicate that the strain S26 forms a branched substrate mycelium that is fragmented at maturity into coccoid and bacillary elements. The aerial mycelium of S26 forms a spore chain surrounded by a spiny sheath (Figure 3), and this micromorphology is typical of strains belonging to the species of *Saccharopolyspora erythraea* [35]. In addition, other sim-

ilarities have been noted between the strain S26 and the species *Saccharopolyspora erythraea*, such as the use of different carbon sources by the isolate S26 being perfectly the same as that of the species *Saccharopolyspora erythraea*, except for the raffinose and the cellulose, which are not used by strain S26 (Supplementary Table S3 and Figure S1C). Furthermore, both strain S26 and the closest species, *Saccharopolyspora erythraea*, secreted a bright red soluble pigment, and they do not produce melanoid pigments (Supplementary Figure S1A). However, some macromorphological differences between S26 and *Saccharopolyspora erythraea* have been noted. In fact, the aerial mycelium of S26 is beige-brown, whereas it is usually white to pink for the species *Saccharopolyspora erythraea* [36]. More characteristics of strain S26 can be found in Supplementary Table S3.

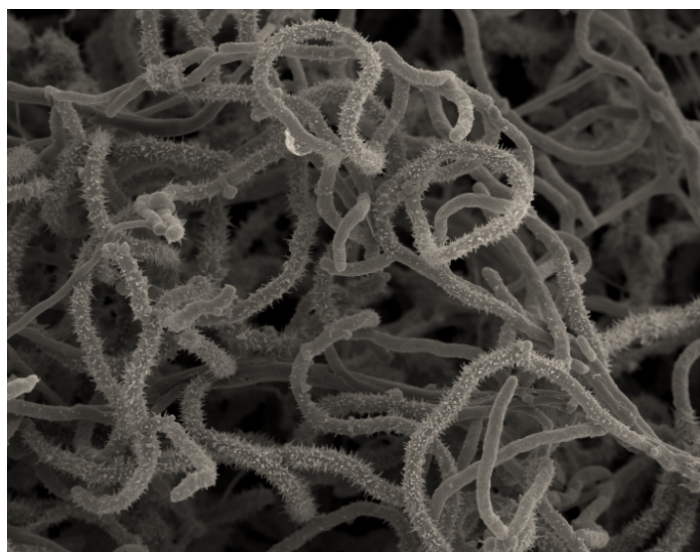


Figure 3. Micromorphology of aerial mycelium, seen by scanning electron microscopy, of isolate S26 showing spore chains surrounded by a spiny sheath. Scale: 200 nm.

On the basis of the genotypic and phenotypic data, we can conclude that the isolate S26 is identical to the species *Saccharopolyspora erythraea*. The 16S rRNA gene sequences of the strain S26, were deposited in GenBank under the accession number OQ567772.

2.5. Biosynthesis and Characterization of Silver Carbonate Nanoparticles

The present study aimed to describe a feasible and simple green method, involving the use of marine *Actinobacteria* for the biosynthesis of $\text{BioAg}_2\text{CO}_3\text{NPs}$, which can be used to overcome the microbial resistance toward antimicrobial agents.

2.5.1. Biosynthesis of Silver Carbonate Nanoparticles

Saccharopolyspora erythraea S26 strain was selected from among 19 active marine actinomycete strains, for the biosynthesis of $\text{BioAg}_2\text{CO}_3\text{NPs}$ because it showed potent antimicrobial activity against various tested microorganisms.

The biosynthesis of $\text{BioAg}_2\text{CO}_3\text{NPs}$ by strain S26 has been primarily identified via color change; the results are shown in Supplementary Figure S2.

The results indicated that, before the addition of the precursor, silver nitrate (AgNO_3), the flask containing the biomass of strain S26 was off-white. Once the AgNO_3 was added, the color changed to dark brown (Supplementary Figure S2). This color change was the first indication of the formation of $\text{BioAg}_2\text{CO}_3\text{NPs}$ by the biomass of strain *Saccharopolyspora erythraea* S26 [37]. These findings have been confirmed by DRX, XRF, and FTIR.

2.5.2. Characterization of Silver Carbonate Nanoparticles

Different characterization techniques, such as Fourier Transform Infrared Spectroscopy (FTIR), X-ray fluorescence (XRF), X-ray diffraction (XRD), scanning electron microscopy

(SEM), and atomic force microscopy (AFM), were employed to confirm the formation of silver carbonate nanoparticles by the biomass of strain S26 and analyze their properties.

2.5.3. FTIR and XRF Analysis of Silver Carbonate Nanoparticles

FTIR and XRF analyses were conducted for the silver carbonate nanoparticles synthesized using the biomass of strain S26. The results are presented in Figure 4 and Table 1.

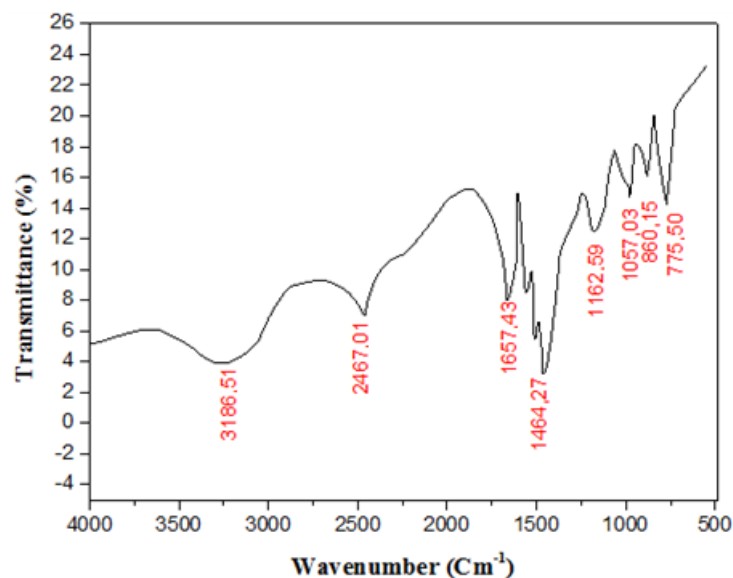


Figure 4. The FTIR spectrum of BioAg₂CO₃NPs synthesized using the biomass of *Saccharopolyspora erythraea* S26 strain.

The FTIR spectrum is a valuable tool for identifying functional groups and chemical bonds. According to the FTIR spectrum presented in Figure 4, four characteristic absorption bands appeared at four different positions, namely 775.50 cm⁻¹, 860.15 cm⁻¹, 1162.59 cm⁻¹, and 1464.27 cm⁻¹, which are attributed to the carbonate groups (CO₃²⁻) in BioAg₂CO₃NPs [38,39]. Therefore, the FTIR spectrum (Figure 4) conveniently demonstrates the presence of CO₃²⁻, within the nanoparticles biosynthesized by the biomass of strain S26. In addition, the IR spectrum of BioAg₂CO₃NPs exhibited peaks at 3186.51 cm⁻¹ and 2467.01 cm⁻¹, corresponding to OH and N–H vibrations, respectively. These peaks indicate the presence of a surface-bound bio-organic phase that acts as a capping/stabilizing agent on the surface of the synthesized nanoparticles [40]. These organic agents have a significant impact on the chemical, physical, and biological features of the nanoparticles [41].

From the results presented in Table 1, which show the atomic content of the BioAg₂CO₃NPs, it is evident that the synthesized nanoparticles predominantly contain silver as a major component in their composition, which aligns with the expected composition of silver carbonate nanoparticles. Therefore, the presence of carbonate groups (CO₃²⁻) and silver atoms in the composition of the synthesized nanoparticles, as indicated in Figure 4 and Table 1, respectively, offers valuable insights into the chemical makeup of the metallic particles, and suggests the successful synthesis of BioAg₂CO₃NPs, utilizing the biomass of strain S26. This compositional information has been further supported by XRD characterization of the synthesized nanoparticles.

Table 1. The atomic content of the BioAg₂CO₃NPs.

Element	ppm	+/-	±2σ
Mo	<LOD	:	7.792
Zr	<LOD	:	6.722
Sr	<LOD	:	5.530
U	<LOD	:	12.946
Rb	<LOD	:	6.935
Th	<LOD	:	10.550
Pb	<LOD	:	16.316
Au	<LOD	:	16.402
Se	<LOD	:	12.140
As	<LOD	:	12.232
Hg	<LOD	:	31.519
Zn	<LOD	:	24.793
W	<LOD	:	83.775
Cu	<LOD	:	50.723
Ni	<LOD	:	45.288
Co	<LOD	:	24.146
Fe	<LOD	:	91.363
Mn	<LOD	:	112.081
Ag	24,072.557	+/-	123.126
Ca	344.031	+/-	40.808
K	132.124	+/-	67.157
S	<LOD	:	250.576
Ba	<LOD	:	39.464
Cs	<LOD	:	9.806
Te	<LOD	:	25.027
Sb	<LOD	:	12.620
Sn	<LOD	:	63.174
Cd	<LOD	:	27.604

2.5.4. XRD Characterization of the Silver Carbonate Nanoparticles

The X-ray diffraction (XRD) analysis was performed in order to examine the crystallographic structure as well as to determine the size of BioAg₂CO₃NPs synthesized using the biomass of strain S26. The obtained results are shown in Figure 5.

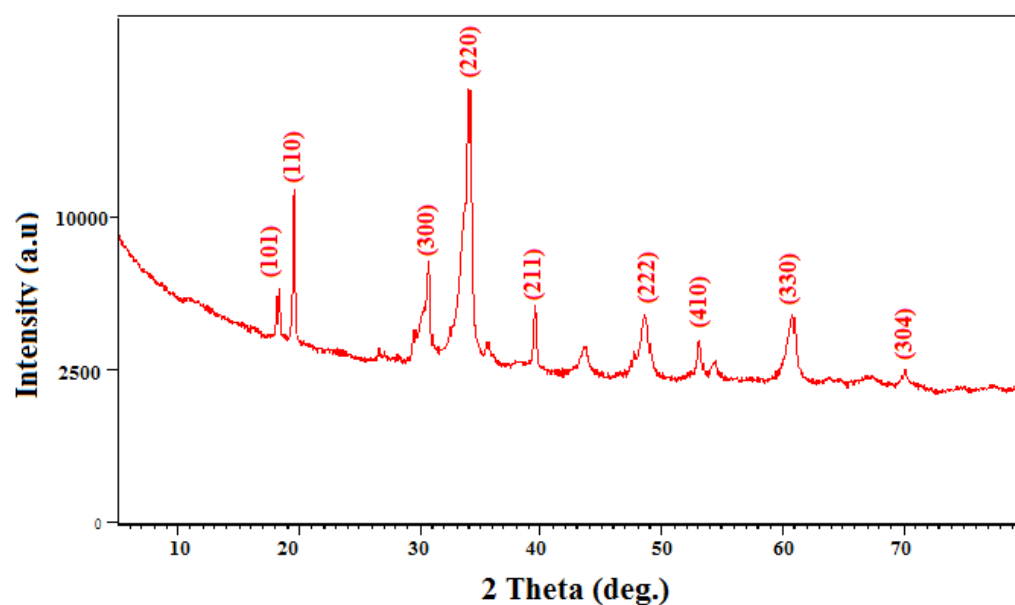


Figure 5. XRD pattern of silver carbonate nanoparticles (Ag₂CO₃NPs) synthesized using the biomass of strain *Saccharopolyspora erythraea* S26.

The diffraction pattern of the BioAg₂CO₃NPs, as depicted in Figure 5, exhibits clearly defined peaks. The distinct diffraction peaks corresponding to the 2θ values recorded in Supplementary Table S4, show well-matched positions and intensities when compared with the standard ICDD files no. 00-031-1237. This similarity strongly suggests that the sample is primarily made of silver carbonate nanoparticles in the hexagonal phase.

The identification of the silver carbonate nanoparticles in the hexagonal phase at high concentrations also raises questions regarding their size. A thorough investigation using the Williamson–Hall plot [42] (Figure 6) is warranted to gain insights into the crystallite size and lattice strain of the biosynthesized BioAg₂CO₃NPs nanoparticles from X-ray diffraction data.

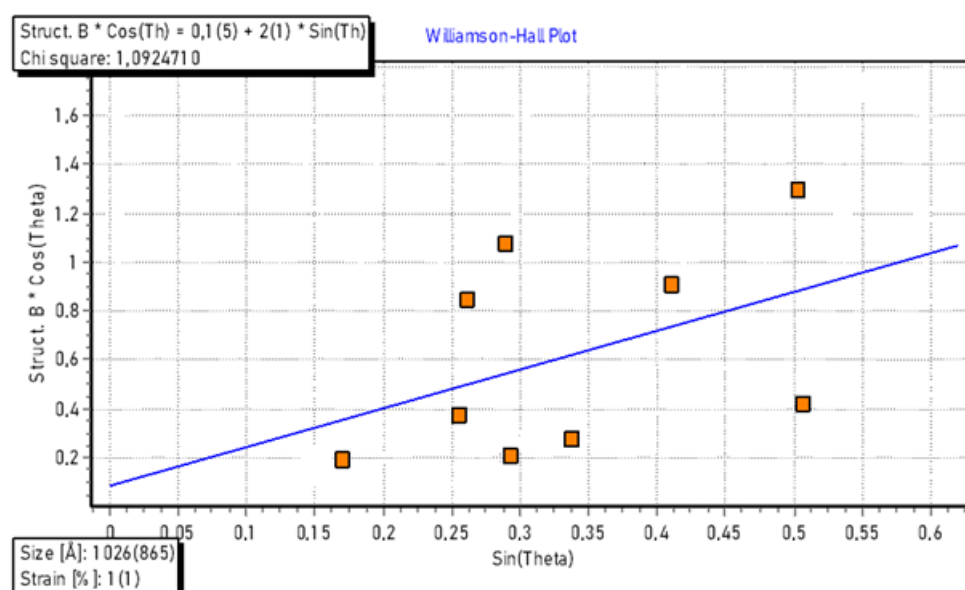


Figure 6. The Williamson–Hall plot of the BioAg₂CO₃NPs nanoparticles.

The strain was assumed to be uniform in all crystallographic directions. The plots showed a slight positive strain present in the BioAg₂CO₃NPs. This strain might be due to lattice expansion. Moreover, the extracted data from the plot clearly indicate that the average crystallite size of the BioAg₂CO₃NPs is 103 nm. A previous study conducted by Loncarevic et al., (2017) [43], reported the synthesis of rod-like Ag₂CO₃ nanoparticles in water through a precipitation reaction between NaHCO₃ and AgNO₃, in the presence of polyvinylpyrrolidone, with a size range from 20 to 50 nm.

The synthesis of silver carbonate nanoparticles has been previously accomplished through a range of physical and chemical methods [43–46]. However, in comparison to these traditional synthesis techniques, the green synthesis of silver carbonate nanoparticles (BioAg₂CO₃NPs) stands out due to its simplicity, cost-effectiveness, non-toxicity, and environmentally friendly nature. Nevertheless, there is a lack of available literature on the green synthesis of silver carbonate nanoparticles so far, and this study can be regarded as the pioneer in reporting the green synthesis of this nanomaterial using a marine strain.

In addition, the inclusion of CO₃^{2−} ions into silver carbonate nanoparticles enhances their biocompatibility, biodegradability, stability, chemical reactivity, and biological activity [47,48]. In fact, in comparison to numerous other inorganic materials, the presence of CO₃^{2−} ions can facilitate nanoparticles' interaction with biological systems, which can potentially reduce toxicity and enhance compatibility with living organisms, this renders them particularly suitable for medical applications [47–49].

2.5.5. Microscopic Characterization of the Silver Carbonate Nanoparticles

Different microscopic methods, including scanning electron microscopy (SEM) and atomic force microscopy (AFM), were utilized to examine the morphology, size, and surface

topology of the silver carbonate nanoparticles synthesized using the biomass of strain S26. The results are illustrated in Figure 7.

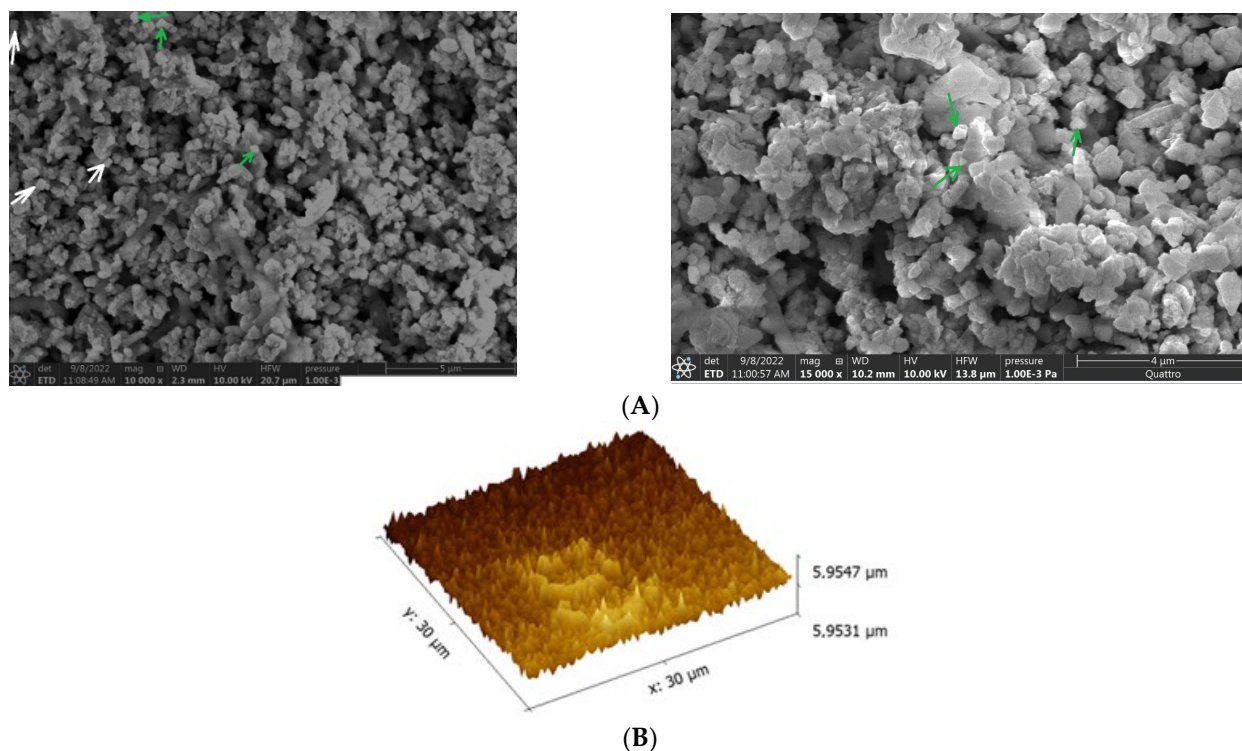


Figure 7. Scanning electron microscope (A) and atomic force microscopy (AFM) (B), of $\text{BioAg}_2\text{CO}_3\text{NPs}$ synthesized from the biomass of strain *Saccharopolyspora erythraea* S26. Green arrow: $\text{BioAg}_2\text{CO}_3\text{NPs}$ with triangular shape, white arrow: $\text{BioAg}_2\text{CO}_3\text{NPs}$ with rectangular shape.

Microscopic analysis through SEM of silver carbonate nanoparticles biosynthesized using the biomass of strain S26 unveiled diverse morphological shapes and uniform distribution, with only a minor presence of particle aggregation (Figure 7A). The prevalent form observed was triangular (indicated by the green arrow) (Figure 7A), while other shapes, such as rectangular (indicated by the white arrow) and spherical, were also detected (Figure 7A). Moreover, the SEM results indicated that the average size of $\text{BioAg}_2\text{CO}_3\text{NPs}$ ranges from 90 nm to 110 nm, thus confirming the findings from the X-ray diffraction data (Figure 6). Various parameters, including the preparation process, the strain used for synthesis, and the culture conditions such as pH and temperature, exert a significant influence on the morphology and size of the synthesized nanoparticles [50].

Atomic force microscopy (AFM) was used to provide a precise three-dimensional representation of the surface topology of the silver carbonate nanoparticles biosynthesized using the biomass of strain S26. The results indicate that the surface topology of the $\text{BioAg}_2\text{CO}_3\text{NPs}$ displayed a triangular shape, as revealed by the AFM findings (Figure 7B). It is important to highlight that the geometrical shape directly affects various attributes, including surface area, optical properties, catalytic activity, as well as their interactions with surrounding environments, such as biological systems [51–53].

2.6. Biological Activity of Silver Carbonate Nanoparticles

2.6.1. Antimicrobial Activity

The antibacterial activity of $\text{BioAg}_2\text{CO}_3\text{NPs}$ was evaluated against a range of pathogenic bacteria and fungi using the agar well diffusion method. Furthermore, the minimum inhibitory concentration (MIC) against the same tested microorganisms was determined through the serial dilution method. The results are presented in Table 2.

Table 2. Antimicrobial activity of BioAg₂CO₃NPs tested against different microorganisms.

Tested Strains	<i>P. aeruginosa</i>	<i>M. luteus</i>	<i>B. subtilis</i>	<i>S. aureus</i>	<i>K. pneumoniae</i>	<i>E. coli</i>	<i>C. albicans</i>
Inhibition zone diameters (mm)							
BioAg ₂ CO ₃ NPs	14	18.50	21	16	11	15	18
Minimum inhibitory concentration (µg/mL)							
BioAg ₂ CO ₃ NPs	37.5	18.75	4.68	37.5	150	37.5	18.75
Oxytetracycline	1.66	2.08	2.08	0.52	1.66	3.33	n.a
Nystatine	n.a	n.a	n.a	n.a	n.a	n.a	n.a

Positive control: oxytetracycline, nystatin; n.a: No activity.

Based on the results presented in Table 2, it is clear that the BioAg₂CO₃NPs synthesized by strain S26 exhibited notable antibacterial activity against the full range of examined pathogens, with inhibition diameters ranging from 11 mm to 21 mm (Supplementary Figure S3). The MIC of nanoparticles synthesized using the biomass of strain S26 was subsequently assessed against each of the tested microorganisms, as detailed in Table 2. The results demonstrate that BioAg₂CO₃NPs are efficient antibacterial agents against all tested microbes, with MIC values ranging from 18.75 to 150 µg/mL. The biological activity of nanoparticles is significantly influenced by their characteristics. Several studies have shown that the size of nanoparticles and their antibacterial activity are inversely correlated; in other words, the smaller the nanoparticle size, the greater the surface interaction area with microbial cells, resulting in heightened antimicrobial activity. [54,55]. Additionally, the antimicrobial potential of BioAg₂CO₃NPs is also shape-dependent [56]. In this context, Pal et al. (2007) [57] found that triangular silver nanoparticles were more effective against *E. coli* compared to spherical nanoparticles.

The vulnerability observed in the tested bacteria and fungi towards BioAg₂CO₃NPs can be attributed to the nanoparticles' ability to attack microbial cells simultaneously through multiple mechanisms, including protein inactivation, the production of reactive oxygen species (ROS) [58], and the formation of free radicals [59]. Consequently, pathogenic microorganisms become incapable of developing resistance to BioAg₂CO₃NPs, unlike traditional chemical antimicrobial agents, such as antibiotics and antifungals, which act on microbial cells via only one mechanism. Due to this rarity of microorganisms' resistance to BioAg₂CO₃NPs, the use of these nanoparticles offers a potential alternative to overcoming multidrug-resistant microorganisms [60,61].

2.6.2. Antibiofilm Activity

The microtiter dish biofilm formation assay was conducted to evaluate and assess the antibiofilm activity of BioAg₂CO₃NPs against the biofilm formed by *Klebsiella pneumoniae* kp6 strain. The experiment was performed in the presence of BioAg₂CO₃NPs, with a final concentration of 150 µg/mL, corresponding to the MIC determined against the kp6 strain (Table 2). The results can be found in Figure 8 and Supplementary Figure S4.

The capacity of BioAg₂CO₃NPs to remove the biofilm formed over 24 h by *Klebsiella pneumoniae* kp6 strain was initially assessed through a visual comparison between the wells treated with BioAg₂CO₃NPs and those of the negative control (wells without BioAg₂CO₃NPs). A clear decrease in the color intensity of crystal violet was observed in wells exposed to BioAg₂CO₃NPs, suggesting good antibiofilm activity against the biofilm formed by the *Klebsiella pneumoniae* kp6 strain (Supplementary Figure S4).

In order to quantify the anti-biofilm activity of BioAg₂CO₃NPs, UV-vis spectroscopy was performed. The results are presented in Figure 8.

As illustrated in Figure 8, the BioAg₂CO₃NPs synthesized using the biomass of strain S26 successfully eradicated 58% of the biofilm formed by the *Klebsiella pneumoniae* kp6 strain, confirming then the good antibiofilm activity of BioAg₂CO₃NPs, observed in Supplementary Figure S4. Several authors have extensively investigated the efficacy of silver nanoparticles (AgNPs) in eliminating biofilms formed by various bacterial strains, however,

to the best of our knowledge, this study was the pioneering investigation aimed to evaluate the antibiofilm activity of silver carbonate nanoparticles against the biofilm formed by *Klebsiella pneumoniae* kp6 strain.

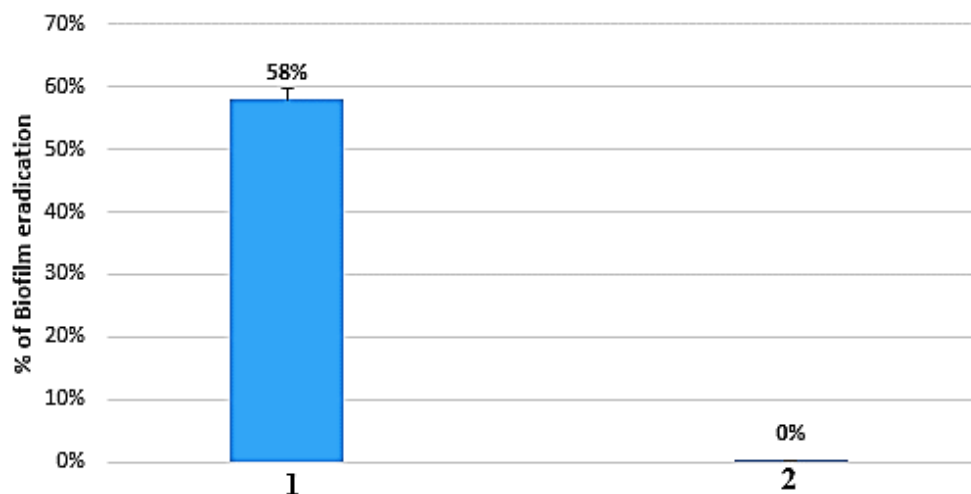


Figure 8. Antibiofilm activity of silver carbonate nanoparticles prepared from biomass of strain S26 against 24 h biofilm formed by *Klebsiella pneumoniae* kp6 strain. 1: BioAg₂CO₃NPs; 2: Control.

The antibiofilm activity of BioAg₂CO₃NPs can be attributed to several mechanisms, including the inhibition of bacterial cell adhesion to the support surface [62], disruption of intermolecular forces [5], and inhibition of Quorum Sensing [63]. Additionally, BioAg₂CO₃NPs may potentially contribute to neutralizing EPS production, which represents the adhesive substance necessary for biofilm formation [64].

Furthermore, the size and shape of nanoparticles significantly influence their antibiofilm activity. Smaller nanoparticles exhibit higher antibiofilm activity, as their diminutive size allows them to penetrate biofilms and adhere to cell membranes, thereby interfering with permeability and metabolism [64,65]. Additionally, rod-shaped nanoparticles have demonstrated superior antibiofilm activity compared to spherical ones [66,67].

3. Materials and Methods

3.1. Sampling of Algae, Sponge, and Marine Sediment

Different samples of algae, marine sponge, and marine sediment were collected at depths ranging from 2 m to 15 m, in two Algerian littoral regions: Ain El-Turck (15 km from the north-west of Oran Province, Algeria) and El-Kala (20 km from the northeast of El Tarf Province, Algeria). The algae was identified as *Codium bursa*, while the marine sponge was identified as *Chondrosia reniformis* (Supplementary Figure S5).

3.2. Isolation of Actinomycetes from the Marine Source

Prior to isolating actinobacteria, marine sediment samples were initially air-dried at room temperature. Subsequently, 1 g of sediment sample was diluted in 9 mL of distilled water, and serial dilutions were conducted from this stock solution until reaching 10⁻³. However, the marine sponge *Chondrosia reniformis* and the algae *Codium bursa*, first underwent an initial surface decontamination using 70% alcohol to eliminate loosely attached microorganisms. Afterward, the samples were cut into small pieces of 1 cm³ using a sterile scalpel and then aseptically ground using sterile pestles and mortars. In total, 10 g of each sample was suspended, separately, in 10 mL of sterile distilled water, from which a serial dilution was prepared. Aliquots (0.1 mL) of each dilution, prepared from different samples, were spread in duplicate on the surface of four culture media: ISP2: glucose 4 g/L, yeast extract 4 g/L, malt extract 10 g/L, agar 12 g, seawater 1 L, pH 7.2 ± 0.2. Casein starch agar (CSA): starch 10 g/L, casein 0.3 g/L, K₂HPO₄ 2 g/L, KNO₃ 2 g/L, NaCl 2 g/L,

MgSO₄·7H₂O 0.05 g/L, CaCO₃ 0.02 g/L, FeSO₄·7H₂O 0.01 g/L, agar 15 g/L, seawater 1 L, pH 7.2 ± 0.2. M4: chitin 2 g/L, agar 18 g/L, seawater 1 L, pH 7.2 ± 0.2. M2: glycerol 6 mL, arginine 1 g/L, K₂HPO₄ 1 g/L, MgSO₄ 0.5 g/L, agar 18 g/L, seawater 1 L, pH 7.2 ± 0.2. To prevent fungal growth, 50 µg/mL of cycloheximide was added to the four used media. Actinomycetes colonies were picked based on their morphological characteristics and then purified to achieve pure cultures.

3.3. Antimicrobial Activity

3.3.1. Preparation of Suspensions

A total of seven bacteria were employed as test microorganisms, including four Gram-positive bacteria: *Staphylococcus aureus* (ATCC 25923), *Bacillus cereus* (ATCC 10876), *Listeria monocytogenes* (ATCC 35152), and *Micrococcus luteus* (ATCC), and three Gram-negative bacteria: *Pseudomonas aeruginosa* (ATCC 19606), *Escherichia coli* (ATCC 25922), and *Klebsiella pneumoniae* (ATCC 70603), in addition to one yeast: *Candida albicans* (ATCC 10231). The tested bacteria and yeast were inoculated into a brain–heart infusion broth and Sabouraud broth, respectively. After 24-h incubation, the turbidity of each culture was adjusted to 0.5 McFarland, after which, the cultures were inoculated onto Müller Hinton agar plates using sterile cotton swabs.

3.3.2. Screening of Antimicrobial Activity Using the Agar Piece Method

To evaluate the antimicrobial potential of actinobacteria isolates, the strains were inoculated onto 5333 media: starch 15 g/L, yeast extract 4 g/L, MgSO₄ 0.5 g/L, K₂HPO₄ 1 g/L, agar 18 g/L, seawater 1 L. After 14 days of incubation at 30 °C, agar cylinders of 6 mm diameter, were cut from the well-grown cultures of actinobacteria isolates and then placed onto pre-seeded Müller Hinton agar plates, containing the target microorganisms. The plates were placed at 4 °C for 4 h to ensure a good diffusion of bioactive metabolites secreted by actinomycete strains, followed by incubation at 37 °C for 24 h for the tested bacteria, and 30 °C for 48 h for the tested yeast [26].

3.4. Molecular Identification and Partial Taxonomic Characterization of Selected Strain

3.4.1. Molecular Identification

The actinomycete isolates demonstrating significant antimicrobial activity were selected for molecular identification through 16S rRNA gene region sequencing. The DNA extraction was performed after the culture of actinomycetes isolates in ISP2 medium: malt extract 10 g/L, yeast extract 4.0 g/L, glucose 4.0 g/L, agar 12 g/L, seawater 1 L). The cultures were incubated at 30 °C for 5 days and 150 rpm. Subsequently, the biomass was harvested with centrifugation at 6000 rpm/min, and then DNA extraction was carried out from the biomass using a Spin Plant Mini Kit (Invisorb, Berlin, Germany). However, the amplification of the 16S rRNA gene region was conducted with PCR using two universal primers, such as 27F and R1492 [68]. The PCR reaction was conducted within microtubes of 200 µL, which contained 50 µL total reaction volume formed by: 22 µL of PCR water, 25 µL of JumpStar Ready Mix (JSRM, Sigma-Aldrich, Berlin, Germany), 1 µL forward primer, and 1 µL reverse primer, as well as 1 µL of template DNA. One tube, without DNA, was used as a control. The PCR reaction was performed in a Mastercycler Gradient (Eppendorf, Germany). The PCR products were purified with NucleoSpin® Gel and PCR Clean-up-Kit (Macherey Nagel, Düren, Germany), and then recovered in 30 µL of elution buffer. The success of PCR was verified through 0.8% agarose gel electrophoresis for 50 min at 70 V in TAE buffer. The partial sequencing of the 16S rRNA gene of actinomycetes strains was accomplished with two primers, F27 and R518. The quality of the resulting sequences was checked manually using the Bioedit alignment program. Furthermore, the obtained sequences were aligned and compared with those available on the GenBank database (<http://www.ncbi.nlm.nih.gov/BLAST>, accessed on 10 March 2023). The phylogenetic tree was calculated with the software MEGA 7, using the neighbor-joining method [69,70].

The resulting tree topologies were evaluated using the bootstrap resampling method of 1000 replicates [71].

3.4.2. Partial Characterization of Selected Strain

Partial taxonomic characterization was conducted on the most potent strain. This involved morphological, physiological, and biochemical characterization following the methods described by [72,73].

3.5. Silver Carbonate Nanoparticle Biosynthesis, Characterization, and Biological Activity Evaluation

3.5.1. Biosynthesis of Silver Carbonate Nanoparticles

One piece of 1 cm³ was cut from a 14-day-old culture of the selected strain and then inoculated into an Erlenmeyer flask (250 mL) containing 100 mL of ISP2 medium. After 5 days of incubation at 30 °C in a shaker (120 rpm), the biomass was separated from the supernatant by centrifugation at 5000 rpm for 30 min. The collected biomass was subsequently subjected to two to three washes to eliminate the residual medium components adhered to the cells [74]. A 2 g portion from the obtained biomass of the selected strain, was suspended in a 250 mL Erlenmeyer flask containing 50 mL of silver nitrate (AgNO₃) and 50 mL of calcium carbonate (CaCO₃) solutions. Both solutions were prepared with an equal concentration of 500 mM in distilled water. Following a 72-h incubation period in the dark at 30 °C and under agitation (150 rpm), the biosynthesis of silver carbonate nanoparticles (BioAg₂CO₃NPs) was visually detected by observing a color shift from the initial pale yellow (the color of the biomass post-washing) to a dark brown.

The biosynthesized BioAg₂CO₃NPs were isolated from the biomass through ultrasonic disruption at 30 °C for 30 min, followed by high-speed centrifugation (18,000 × g for 30 min). Subsequently, the collected BioAg₂CO₃NPs were dried at 100 °C [75].

3.5.2. Characterization of Synthesized Silver Carbonate Nanoparticles

The characterization step of the synthesized BioAg₂CO₃NPs by the selected strain, aimed to gain a comprehensive understanding of their properties, composition, morphology, and size. To achieve this, the synthesized pellets of BioAg₂CO₃NPs were dispersed in sterile double-distilled water and centrifuged for 10 min at 10,000 rpm. The nanoparticle pellets were dried at 50 °C and were analyzed by X-ray diffraction (XRD) (Malvern Panalytical, Empyreon, Malvern, UK). To conduct elemental analysis of the BioAg₂CO₃NPs, biosynthesized by the selected *Actinobacteria* strain, the X-ray fluorescence (XRF) technique, was employed through a Thermo Scientific Niton™ XL3t 106399 XRF Analyzer (Billerica, MA, USA). The capping and stabilizing agent present in the surface of the BioAg₂CO₃NPs were analyzed by FTIR in the range of 400–4000 cm⁻¹ at a resolution of 4 cm⁻¹ using Tensor II, Bruker, (Billerica, MA, USA). The morphology of the biosynthesized nanoparticles was determined using scanning electron microscopy (ThermoFisher Scientific, Quattro, (Billerica, MA, USA), as well as the Atomic Force Microscope (AFM).

3.5.3. Biological Activity Determination of Silver Carbonate Nanoparticles Antimicrobial Activity

The agar well diffusion method was used to evaluate the antimicrobial activity of the BioAg₂CO₃NPs, synthesized using the biomass of the selected strain, against a panel of seven pathogenic microorganisms. However, the serial dilution method in 96-well microtiter plates was applied to determine the minimum inhibitory concentration (MIC) of BioAg₂CO₃NPs, against the tested microorganisms [74].

After the adjustment of microbial culture turbidity for each tested bacteria and yeast to 0.5 McFarland, the microbial suspension was inoculated onto the surfaces of Muller Hinton and Sabouraud medium, for bacteria and yeast, respectively. Afterward, wells with a diameter of 6 mm, were created in each Petri dish using a sterile cork borer. Subsequently, 20 µL of silver carbonate nanoparticle solution, prepared at a concentration of 150 µg/mL,

was introduced into each well. The plates were incubated for 24 h at 30–37 °C, following the incubation of plates, the inhibition areas were measured [76].

The minimum inhibitory concentration (MIC) of BioAg₂CO₃NPs was determined using the serial dilution method in 96-well microtiter plates. The BioAg₂CO₃NPs synthesized using the biomass of the selected strain were tested against pathogenic microorganisms at final concentrations ranging from 150 µg/mL to 1.17 µg/mL, with distilled water used as the negative control. After incubation, the minimum inhibitory concentration (MIC) was determined as the lowest concentration visibly inhibiting the growth of each tested microorganism [77].

Antibiofilm Activity

Polystyrene 96-well microtiter plates were used to test the efficiency of BioAg₂CO₃NPs, prepared from the biomass of the selected strain, to eradicate the 24-h biofilm formed by *Klebsiella pneumoniae* kp6 strain. The strain used in this experience was isolated from urinary catheter and endotracheal tubes from the services of Intensive Care, Urology, and Neurology, at the University Hospital of Tlemcen. This strain was a high biofilm producer on inert surfaces as described previously by [78].

Each well of the microtiter plate was filled with 200 µL suspensions of *Klebsiella pneumoniae* kp6, adjusted to a turbidity of 0.5 McFarland. After incubation for 24 h at 37 °C, the non-adherent cells were gently removed by washing the biofilms three times with distilled water [79]. Simultaneously, the suspension of BioAg₂CO₃NPs was prepared at a concentration equivalent to the MIC determined against the *Klebsiella pneumoniae* ATCC 70603 strain. Then, 200 µL of this suspension was added to each well of the microtiter plate. After 24 h of incubation at 37 °C, the wells were rinsed three times, using distilled water. Afterward, the biofilm was stained with 200 µL of 0.1% crystal violet for 15 min, washed with tap water to remove excess stain, and then allowed to dry.

To quantify microbial adhesion, the stain in the wells was diluted with 200 µL acetic acid in water (33%), and the absorbance was measured at 595 nm with a microplate reader. Percentages of reduction in biofilm structures were calculated using the formula [79]:

$$\text{Biofilm inhibition (\%)} = [(OD \text{ control} - OD \text{ sample}) / OD \text{ control}] \times 100$$

4. Conclusions

The present study represents the first attempt at the green synthesis of low-cost and eco-friendly silver carbonate nanoparticles using the biomass of the marine strain *Saccharopolyspora erythraea* S26, isolated from the Algerian coastline. The synthesized nanoparticles primarily exhibited a triangular morphology, with sizes ranging from 90 to 110 nm. Additionally, the synthesized BioAg₂CO₃NPs displayed good antibacterial and antibiofilm activity. These findings suggest that BioAg₂CO₃NPs can serve as an alternative approach to overcome microbial resistance to various antimicrobial agents since microbial resistance toward metallic nanoparticles is extremely rare.

Supplementary Materials: The following supporting information can be downloaded at: <https://www.mdpi.com/article/10.3390/md21100536/s1>, Figure S1: A. Colony description and melanin pigment formation; from top left to bottom right: ISP2, ISP3, ISP4, ISP5, ISP6 and ISP7. B. Sodium chloride tolerance test; [NaCl] from top left to bottom right: 0%, 2.5%, 5%, 7.5%, 10%. C. Carbon utilization test; from top left to bottom right: glucose, arabinose, sucrose, xylose, inositol, mannose, fructose, rhamnose, raffinose, cellulose, water); Figure S2: Biosynthesis of silver carbonate nanoparticles by the biomass of *Saccharopolyspora erythraea* S26 strain; Figure S3: Antimicrobial activity of silver carbonate nanoparticles prepared from the biomass of strain *Saccharopolyspora erythraea* S26; Figure S4: Microtiter plate biofilm assay for the evaluation of the antibiofilm activity of BioAg₂CO₃NPs against the biofilm formed by strain *Klebsiella pneumoniae* kp6 strain; Figure S5: Marine samples used for Actinobacteria isolation. A: Marine algae *Codium bursa*; B: Marine sponge *Chondrosia reniformis*; Table S1: Antimicrobial activity (mm) of Actinobacteria strains against different pathogenic microorganism; Table S2: Molecular identification of the 18 selected active strains,

based on 16S rRNA gene sequencing; Table S3: Characteristics of the S26 strain and the closest species within the genus *Saccharopolyspora*. 1. S26; 2. *Saccharopolyspora erythraea* DSM 40517T (AM420293). 3. *Saccharopolyspora spinosporotrichia* DSM 44350T (Y09571). Table S4: Peak list of silver carbonate nanoparticles biosynthesis using the biomass strain S26.

Author Contributions: Conceptualization, O.M. and I.B.; methodology, A.A.; software, Y.K. (Yasmina Khane); validation, S.A., G.M.S. and M.M.S.-B.; formal analysis, K.H.; investigation, S.G.; resources, M.M.S.; data curation, A.Z.; writing—original draft preparation, I.M.; writing—review and editing, Y.K. (Yacine Kerchich); visualization, F.B.; supervision, O.M.; project administration, M.B.; funding acquisition, O.M. All authors have read and agreed to the published version of the manuscript.

Funding: The authors would like to extend their sincere appreciation to the Researchers Supporting Project Number (RSPD2023R986), King Saud University, Riyadh, Saudi Arabia.

Institutional Review Board Statement: Not applicable.

Data Availability Statement: Not applicable.

Acknowledgments: The authors are grateful to the Center for Scientific and Technical Research in Physicochemical Analysis (PTAPC-Laghouat-CRAPC), Algeria, for performing DRX and MEB analysis. The authors would like to thank the General Directorate of Research and Technology Development, Ministry of Higher Education, and Scientific Research of Algeria for supporting this work. Special thanks to Said Maabed for their invaluable contribution to the interpretation of XRD data. The authors thank the support of University of Misan and University of Technology, Iraq. Also, the authors would like to extend their sincere appreciation to the Researchers Supporting Project Number (RSPD2023R986), King Saud University, Riyadh, Saudi Arabia.

Conflicts of Interest: The authors declare no conflict of interest.

References

1. Reygaert, W.C. An overview of the antimicrobial resistance mechanisms of bacteria. *AIMS Microbiol.* **2018**, *4*, 482–501. [[CrossRef](#)] [[PubMed](#)]
2. Li, Y.; Xiao, P.; Wang, Y.; Hao, Y. Mechanisms and Control Measures of Mature Biofilm Resistance to Antimicrobial Agents in the Clinical Context. *ACS Omega* **2020**, *5*, 22684–22690. [[CrossRef](#)] [[PubMed](#)]
3. Seo, M.; Oh, T.; Bae, S. Antibiofilm activity of silver nanoparticles against biofilm forming *Staphylococcus pseudintermedius* isolated from dogs with otitis externa. *Vet. Med. Sci.* **2021**, *7*, 1551–1557. [[CrossRef](#)]
4. Zhang, K.; Li, X.; Yu, C.; Wang, Y. Promising Therapeutic Strategies Against Microbial Biofilm Challenges. *Front. Cells Infect. Microbiol.* **2020**, *10*, 359. [[CrossRef](#)]
5. Khudier, M.A.; Hammadi, H.A.; Atyia, H.T.; Al-Karagoly, H.; Albukhaty, S.; Sulaiman, G.M.; Dewir, Y.H.; Mahood, H.B. Antibacterial activity of green synthesized selenium nanoparticles using *Vaccinium arctostaphylos* (L.) fruit extract. *Cogent Food Agric.* **2023**, *9*, 2245612. [[CrossRef](#)]
6. Alzubaidi, A.K.; Al-Kaabi, W.J.; Al Ali, A.; Albukhaty, S.; Al-Karagoly, H.; Sulaiman, G.M.; Asiri, M.; Khane, Y. Green Synthesis and Characterization of Silver Nanoparticles Using *Flaxseed* Extract and Evaluation of Their Antibacterial and Antioxidant Activities. *Appl. Sci.* **2023**, *13*, 2182. [[CrossRef](#)]
7. Alhujaily, M.; Albukhaty, S.; Yusuf, M.; Mohammed, M.K.A.; Sulaiman, G.M.; Al-Karagoly, H.; Alyamani, A.A.; Albaqami, J.; AlMalki, F.A. Recent Advances in Plant-Mediated Zinc Oxide Nanoparticles with Their Significant Biomedical Properties. *Bioengineering* **2022**, *9*, 541. [[CrossRef](#)]
8. Khane, Y.; Benouis, K.; Albukhaty, S.; Sulaiman, G.M.; Abomughaid, M.M.; Al Ali, A.; Aouf, D.; Fenniche, F.; Khane, S.; Chaibi, W.; et al. Green Synthesis of Silver Nanoparticles Using Aqueous *Citrus limon* Zest Extract: Characterization and Evaluation of Their Antioxidant and Antimicrobial Properties. *Nanomaterials* **2022**, *12*, 2013. [[CrossRef](#)] [[PubMed](#)]
9. Messaoudi, O.; Bendahou, M. Biological Synthesis of Nanoparticles Using Endophytic Microorganisms: Current Development. In *“Biological Synthesis of Nanoparticles Using Endophytic Microorganisms: Current Development”* in *Nanotechnology and the Environment*; Sen, M., Ed.; IntechOpen: Rijeka, Croatia, 2020; pp. 1–19. [[CrossRef](#)]
10. Sabido, E.M.; Tenebro, C.P.; Trono, D.J.V.L.; Vicera, C.V.B.; Leonida, S.F.L.; Maybay, J.J.W.B.; Reyes-Salalda, R.; Amago, D.S.; Aguadera, A.M.V.; Octaviano, M.C.; et al. Insights into the Variation in Bioactivities of Closely Related *Streptomyces* Strains from Marine Sediments of the Visayan Sea against ESKAPE and Ovarian Cancer. *Mar. Drugs* **2021**, *19*, 441. [[CrossRef](#)]
11. Messaoudi, O. Isolement et Caractérisation de Nouvelles Molécules Bioactives à Partir D’Actinomycètes Isolées du sol Algérien. Ph.D. Thesis, Université de Tlemcen, Tlemcen, Algeria, 2020.
12. Messaoudi, O.; Sudarman, E.; Bendahou, M.; Jansen, R.; Stadler, M.; Wink, J. Kenalactams A–E, Polyene Macrolactams Isolated from *Nocardioopsis* CG3. *J. Nat. Prod.* **2019**, *82*, 1081–1088. [[CrossRef](#)]

13. Meliani, H.; Makhloufi, A.; Cherif, A.; Mahjoubi, M.; Makhloufi, K. Biocontrol of toxinogenic *Aspergillus flavus* and *Fusarium oxysporum* f. sp. *albedinis* by two rare Saharan actinomycetes strains and LC-ESI/MS-MS profiling of their antimicrobial products. *Saudi J. Biol. Sci.* **2022**, *29*, 103288. [[CrossRef](#)]
14. Fahmy, N.M.; Abdel-Tawab, A.M. Isolation and characterization of marine sponge-associated *Streptomyces* sp. NMF6 strain producing secondary metabolite(s) possessing antimicrobial, antioxidant, anticancer, and antiviral activities. *J. Genet. Eng. Biotechnol.* **2021**, *19*, 102. [[CrossRef](#)]
15. Messaoudi, O.; Sudarman, E.; Patel, C.; Bendahou, M.; Wink, J. Metabolic Profile, Biotransformation, Docking Studies and Molecular Dynamics Simulations of Bioactive Compounds Secreted by CG3 Strain. *Antibiotics* **2022**, *11*, 657. [[CrossRef](#)]
16. Axenov-Gribanov, D.V.; Kostka, D.V.; Vasilieva, U.; Shatilina, Z.M.; Krasnova, M.E.; Pereliaeva, E.V.; Zolotovskaya, E.D.; Morgunova, M.M.; Rusanovskaya, O.O.; Timofeyev, M.A. Cultivable Actinobacteria First Found in Baikal Endemic Algae Is a New Source of Natural Products with Antibiotic Activity. *Int. J. Microbiol.* **2020**, *2020*, 5359816. [[CrossRef](#)]
17. Gerovasileiou, V.; Voultziadou, E. Marine Caves of the Mediterranean Sea: A Sponge Biodiversity Reservoir within a Biodiversity Hotspot. *PLoS ONE* **2012**, *7*, e39873. [[CrossRef](#)]
18. Nnaji, P.T.; Morse, H.R.; Adukwu, E.; Chidugu-Ogboribo, R.U. Sponge–Microbial Symbiosis and Marine Extremozymes: Current Issues and Prospects. *Sustainability* **2022**, *14*, 6984. [[CrossRef](#)]
19. Zhou, J.; Richlen, M.L.; Sehein, T.R.; Kulis, D.M.; Anderson, D.M.; Cai, Z. Microbial Community Structure and Associations During a Marine Dinoflagellate Bloom. *Front. Microbiol.* **2018**, *9*, 1201. [[CrossRef](#)] [[PubMed](#)]
20. Egan, S.; Kumar, V.; Nappi, J.; Gardiner, M. Microbial diversity and symbiotic interactions with macroalgae. In *Algal and Cyanobacteria Symbioses*; World Scientific: Singapore, 2017; pp. 493–546.
21. Ribeiro, I.; Girão, M.; Alexandrino, D.A.M.; Ribeiro, T.; Santos, C.; Pereira, F.; Mucha, A.P.; Urbatzka, R.; Leão, P.N.; Carvalho, M.F. Diversity and Bioactive Potential of Actinobacteria Isolated from a Coastal Marine Sediment in Northern Portugal. *Microorganisms* **2020**, *8*, 1691. [[CrossRef](#)]
22. Wu, J.; Peng, Z.; Guan, T.-W.; Yang, H.; Tian, X. Diversity of actinobacteria in sediments of Qaidam Lake and Qinghai Lake, China. *Arch. Microbiol.* **2021**, *203*, 2875–2885. [[CrossRef](#)] [[PubMed](#)]
23. Huang, Z.; Mo, S.; Yan, L.; Wei, X.; Huang, Y.; Zhang, L.; Zhang, S.; Liu, J.; Xiao, Q.; Lin, H.; et al. A Simple Culture Method Enhances the Recovery of Culturable Actinobacteria from Coastal Sediments. *Front. Microbiol.* **2021**, *12*, 675048. [[CrossRef](#)] [[PubMed](#)]
24. Djinni, I.; Defant, A.; Kecha, M.; Mancini, I. Metabolite profile of marine-derived endophytic *Streptomyces sundarbansensis* WR1158 by liquid chromatography-mass spectrometry and evaluation of culture conditions on antibacterial activity and mycelial growth. *J. Appl. Microbiol.* **2013**, *116*, 39–50. [[CrossRef](#)]
25. Ouchene, R.; Intertaglia, L.; Zaatout, N.; Kecha, M.; Suzuki, M.T. Selective isolation, antimicrobial screening and phylogenetic diversity of marine actinomycetes derived from the Coast of Bejaia City (Algeria), a polluted and microbiologically unexplored environment. *J. Appl. Microbiol.* **2021**, *132*, 2870–2882. [[CrossRef](#)] [[PubMed](#)]
26. Messaoudi, O.; Wink, J.; Bendahou, M. Diversity of *Actinobacteria* Isolated from Date Palms Rhizosphere and Saline Environments: Isolation, Identification and Biological Activity Evaluation. *Microorganisms* **2020**, *8*, 1853. [[CrossRef](#)]
27. Arocha-Garza, H.F.; Canales-Del Castillo, R.; Eguiarte, L.E.; Souza, V.; De la Torre-Zavala, S. High diversity and suggested endemicity of culturable Actinobacteria in an extremely oligotrophic desert oasis. *PeerJ* **2017**, *5*, e3247. [[CrossRef](#)] [[PubMed](#)]
28. Long, Y.; Zhang, Y.; Huang, F.; Liu, S.; Gao, T.; Zhang, Y. Diversity and antimicrobial activities of culturable actinomycetes from *Odontotermes formosanus* (Blattaria: Termitidae). *BMC Microbiol.* **2022**, *22*, 80. [[CrossRef](#)]
29. Messaoudi, O. Contribution à la Caractérisation des Souches D’Actinomycètes Productrice des Métabolites Antibactériennes Isolée de la Sebkhia de Kendasa (Bechar). Master’s Thesis, Université of Tlemcen, Tlemcen, Algeria, 2013.
30. Yuan, M.; Yu, Y.; Li, H.-R.; Dong, N.; Zhang, X.-H. Phylogenetic Diversity and Biological Activity of Actinobacteria Isolated from the Chukchi Shelf Marine Sediments in the Arctic Ocean. *Mar. Drugs* **2014**, *12*, 1281–1297. [[CrossRef](#)]
31. Baig, U.; Dahanukar, N.; Shintre, N.; Holkar, K.; Pund, A.; Lele, U.; Gujarathi, T.; Patel, K.; Jakati, A.; Singh, R.; et al. Phylogenetic diversity and activity screening of cultivable Actinobacteria isolated from marine sponges and associated environments from the western coast of India. *Access Microbiol.* **2021**, *3*, 000242. [[CrossRef](#)]
32. Pimentel-Elardo, S.M.; Kozytska, S.; Bugni, T.S.; Ireland, C.M.; Moll, H.; Hentschel, U. Anti-Parasitic Compounds from *Streptomyces* sp. Strains Isolated from Mediterranean Sponges. *Mar. Drugs* **2010**, *8*, 373–380. [[CrossRef](#)] [[PubMed](#)]
33. Kuang, W.; Li, J.; Zhang, S.; Long, L. Diversity and distribution of Actinobacteria associated with reef coral *Porites lutea*. *Front. Microbiol.* **2015**, *6*, 1094. [[CrossRef](#)]
34. Peraud, O.; Biggs, J.S.; Hughen, R.W.; Light, A.R.; Concepcion, G.P.; Olivera, B.M.; Schmidt, E.W. Microhabitats within Venomous Cone Snails Contain Diverse Actinobacteria. *Appl. Environ. Microbiol.* **2009**, *75*, 6820–6826. [[CrossRef](#)]
35. Lacey, J. Nomenclature of *Saccharopolyspora erythraea* Labeda 1987 and *Streptomyces erythraeus* (Waksman 1923) Waksman and Henrici 1948, and Proposals for the Alternative Epithet *Streptomyces labedae* sp. nov. *Int. J. Syst. Evol. Microbiol.* **1987**, *37*, 458. [[CrossRef](#)]
36. Labeda, D.P. Transfer of the Type Strain of *Streptomyces erythraeus* (Waksman 1923) Waksman and Henrici 1948 to the Genus *Saccharopolyspora* Lacey and Goodfellow 1975 as *Saccharopolyspora erythraea* sp. nov., and Designation of a Neotype Strain for *Streptomyces erythraeus*. *Int. J. Syst. Evol. Microbiol.* **1987**, *37*, 19–22. [[CrossRef](#)]

37. Deka, D.R.; Das, P.; Paul, D.C.; Sarma, M.P. Green synthesis of silver nanoparticles using *Swertia chirayita* leaves and its effect against selected human pathogens. *Int. J. Bot. Stud.* **2022**, *7*, 227–232.
38. Karimkhah, F.; Elhamifar, D.; Shaker, M. Ag₂CO₃ containing magnetic nanocomposite as a powerful and recoverable catalyst for Knoevenagel condensation. *Sci. Rep.* **2021**, *11*, 18736. [[CrossRef](#)] [[PubMed](#)]
39. Cao, R.; Yang, H.; Deng, X.; Zhang, S.; Xu, X. In-situ synthesis of amorphous silver silicate/carbonate composites for selective visible-light photocatalytic decomposition. *Sci. Rep.* **2017**, *7*, 15001. [[CrossRef](#)]
40. Zia, F.; Ghafoor, N.; Iqbal, M.; Mehboob, S. Green synthesis and characterization of silver nanoparticles using *Cydonia oblong* seed extract. *Appl. Nanosci.* **2016**, *6*, 1023–1029. [[CrossRef](#)]
41. Bélteky, P.; Rónavári, A.; Igaz, N.; Szerencsés, B.; Tóth, I.Y.; Pfeiffer, I.; Kiricsi, M.; Kónya, Z. Silver nanoparticles: Aggregation behavior in biorelevant conditions and its impact on biological activity. *Int. J. Nanomed.* **2019**, *14*, 667–687. [[CrossRef](#)]
42. Zak, A.K.; Majid, W.A.; Abrishami, M.; Yousefi, R. X-ray analysis of ZnO nanoparticles by Williamson–Hall and size–strain plot methods. *Solid State Sci.* **2011**, *13*, 251–256. [[CrossRef](#)]
43. Lončarević, D.; Vukoje, I.; Dostanić, J.; Bjelajac, A.; Đorđević, V.; Dimitrijević, S.; Nedeljković, J.M. Antimicrobial and Photocatalytic Abilities of Ag₂CO₃ Nano-Rods. *ChemistrySelect* **2017**, *2*, 2931–2938. [[CrossRef](#)]
44. Buckley, J.J.; Gai, P.L.; Lee, A.F.; Olivi, L.; Wilson, K. Silver carbonate nanoparticles stabilised over alumina nanoneedles exhibiting potent antibacterial properties. *Chem. Commun.* **2008**, *34*, 4013–4015. [[CrossRef](#)]
45. Xie, J.; Fang, C.; Zou, J.; Lu, H.; Tian, C.; Han, C.; Zhao, D. In situ ultrasonic formation of AgBr/Ag₂CO₃ nanosheets composite with enhanced visible-driven photocatalytic performance. *Mater. Lett.* **2016**, *170*, 62–66. [[CrossRef](#)]
46. Lakbita, O.; Rhouta, B.; Maury, F.; Senocq, F.; Amjoud, M.; Daoudi, L. On the key role of the surface of palygorskite nanofibers in the stabilization of hexagonal metastable β-Ag₂CO₃ phase in palygorskite-based nanocomposites. *Appl. Clay Sci.* **2019**, *172*, 123–134. [[CrossRef](#)]
47. Chen, S.; Zhao, D.; Li, F.; Zhuo, R.-X.; Cheng, S.-X. Co-delivery of genes and drugs with nanostructured calcium carbonate for cancer therapy. *RSC Adv.* **2012**, *2*, 1820–1826. [[CrossRef](#)]
48. Sun, B.; Tran, K.K.; Shen, H. Enabling customization of non-viral gene delivery systems for individual cell types by surface-induced mineralization. *Biomaterials* **2009**, *30*, 6386–6393. [[CrossRef](#)]
49. Hanifi, A.; Fathi, M.H.; Sadeghi, H.M.M. Effect of strontium ions substitution on gene delivery related properties of calcium phosphate nanoparticles. *J. Mater. Sci. Mater. Med.* **2010**, *21*, 2601–2609. [[CrossRef](#)] [[PubMed](#)]
50. Haruta, M. Nanoparticulate Gold Catalysts for Low-Temperature CO Oxidation. *ChemInform* **2004**, *7*, 163–172. [[CrossRef](#)]
51. Velmurugan, P.; Lee, S.-M.; Iydropose, M.; Lee, K.-J.; Oh, B.-T. Pine cone-mediated green synthesis of silver nanoparticles and their antibacterial activity against agricultural pathogens. *Appl. Microbiol. Biotechnol.* **2012**, *97*, 361–368. [[CrossRef](#)]
52. Sholkamy, E.N.; Ahamd, M.S.; Yasser, M.M.; Eslam, N. Anti-microbiological activities of bio-synthesized silver Nano-stars by *Saccharopolyspora hirsuta*. *Saudi J. Biol. Sci.* **2018**, *26*, 195–200. [[CrossRef](#)] [[PubMed](#)]
53. Pallavi, S.S.; Rudayni, H.A.; Bepari, A.; Niazi, S.K.; Nayaka, S. Green synthesis of Silver nanoparticles using *Streptomyces hirsutus* strain SNPGA-8 and their characterization, antimicrobial activity, and anticancer activity against human lung carcinoma cell line A549. *Saudi J. Biol. Sci.* **2021**, *29*, 228–238. [[CrossRef](#)]
54. Van Dong, P.; Ha, C.H.; Binh, L.T.; Kasbohm, J. Chemical synthesis and antibacterial activity of novel-shaped silver nanoparticles. *Int. Nano Lett.* **2012**, *2*, 9. [[CrossRef](#)]
55. Raza, M.A.; Kanwal, Z.; Rauf, A.; Sabri, A.N.; Riaz, S.; Naseem, S. Size- and Shape-Dependent Antibacterial Studies of Silver Nanoparticles Synthesized by Wet Chemical Routes. *Nanomaterials* **2016**, *6*, 74. [[CrossRef](#)] [[PubMed](#)]
56. Inam, M.; Foster, J.C.; Gao, J.; Hong, Y.; Du, J.; Dove, A.P.; O'Reilly, R.K. Size and shape affects the antimicrobial activity of quaternized nanoparticles. *J. Polym. Sci. Part A Polym. Chem.* **2018**, *57*, 255–259. [[CrossRef](#)]
57. Pal, S.; Tak, Y.K.; Song, J.M. Does the Antibacterial Activity of Silver Nanoparticles Depend on the Shape of the Nanoparticle? A Study of the Gram-Negative Bacterium *Escherichia coli*. *Appl. Environ. Microbiol.* **2007**, *73*, 1712–1720. [[CrossRef](#)]
58. Dakal, T.C.; Kumar, A.; Majumdar, R.S.; Yadav, V. Mechanistic basis of antimicrobial actions of silver nanoparticles. *Front. Microbiol.* **2016**, *7*, 1831. [[CrossRef](#)] [[PubMed](#)]
59. Kim, J.S.; Kuk, E.; Yu, K.N.; Kim, J.-H.; Park, S.J.; Lee, H.J.; Kim, S.H.; Park, Y.K.; Park, Y.H.; Hwang, C.-Y.; et al. Antimicrobial effects of silver nanoparticles. *Nanomed. Nanotechnol. Biol. Med.* **2007**, *3*, 95–101. [[CrossRef](#)] [[PubMed](#)]
60. Wahab, S.; Khan, T.; Adil, M.; Khan, A. Mechanistic aspects of plant-based silver nanoparticles against multi-drug resistant bacteria. *Heliyon* **2021**, *7*, e07448. [[CrossRef](#)]
61. Franci, G.; Falanga, A.; Galdiero, S.; Palomba, L.; Rai, M.; Morelli, G.; Galdiero, M. Silver Nanoparticles as Potential Antibacterial Agents. *Molecules* **2015**, *20*, 8856–8874. [[CrossRef](#)]
62. Chávez-Andrade, G.M.; Tanomaru-Filho, M.; Bernardi, M.I.B.; Leonardo, R.d.T.; Faria, G.; Guerreiro-Tanomaru, J.M. Antimicrobial and biofilm anti-adhesion activities of silver nanoparticles and farnesol against endodontic microorganisms for possible application in root canal treatment. *Arch. Oral Biol.* **2019**, *107*, 104481. [[CrossRef](#)]
63. Saeki, E.K.; Martins, H.M.; de Camargo, L.C.; Anversa, L.; Tavares, E.R.; Yamada-Ogatta, S.F.; Lioni, L.M.Y.; Kobayashi, R.K.T.; Nakazato, G. Effect of Biogenic Silver Nanoparticles on the Quorum-Sensing System of *Pseudomonas aeruginosa* PAO1 and PA14. *Microorganisms* **2022**, *10*, 1755. [[CrossRef](#)]
64. Joshi, A.S.; Singh, P.; Mijakovic, I. Interactions of Gold and Silver Nanoparticles with Bacterial Biofilms: Molecular Interactions behind Inhibition and Resistance. *Int. J. Mol. Sci.* **2020**, *21*, 7658. [[CrossRef](#)]

65. Galvez, A.M.; Ramos, K.M.; Teja, A.J.; Baculi, R. Bacterial exopolysaccharide-mediated synthesis of silver nanoparticles and their application on bacterial biofilms. *J. Microbiol. Biotechnol. Food Sci.* **2019**, *8*, 970–978. [[CrossRef](#)]
66. Aldujaili, N.H.; Alrufa, M.M.; Sahib, F.H. Antibiofilm antibacterial and antioxidant activity of biosynthesized silver nanoparticles using *Pantoea agglomerans*. *J. Pharm. Sci. Res.* **2017**, *9*, 1220.
67. Al-Wrafy, F.A.; Al-Gheethi, A.A.; Ponnusamy, S.K.; Noman, E.A.; Fattah, S.A. Nanoparticles approach to eradicate bacterial biofilm-related infections: A critical review. *Chemosphere* **2021**, *288*, 132603. [[CrossRef](#)] [[PubMed](#)]
68. Lane, D.J. 6S/23S rRNA Sequencing. In *Nucleic Acid Techniques in Bacterial Systematics*; Stackebrandt, E., Goodfellow, M., Eds.; John Wiley and Sons: New York, NY, USA, 1991; pp. 115–175.
69. Saitou, N.; Nei, M. The neighbor-joining method: A new method for reconstructing phylogenetic trees. *Mol. Biol. Evol.* **1987**, *4*, 406–425. [[CrossRef](#)] [[PubMed](#)]
70. Tamura, K.; Stecher, G.; Peterson, D.; Filipiński, A.; Kumar, S. MEGA6: Molecular Evolutionary Genetics Analysis Version 6.0. *Mol. Biol. Evol.* **2013**, *30*, 2725–2729. [[CrossRef](#)]
71. Felsenstein, J. Confidence limits on phylogenies: An approach using the bootstrap. *Evolution* **1985**, *39*, 783–791. [[CrossRef](#)]
72. Shirling, E.B.; Gottlieb, D. Methods for characterization of *Streptomyces* species. *Int. J. Syst. Evol. Microbiol.* **1966**, *16*, 313–340. [[CrossRef](#)]
73. Williams, S.T.; Goodfellow, M.; Alderson, G.; Wellington, E.M.H.; Sneath, P.H.A.; Sackin, M.J. Numerical Classification of *Streptomyces* and Related Genera. *Microbiology* **1983**, *129*, 1743–1813. [[CrossRef](#)]
74. Messaoudi, O.; Steinmann, E.; Praditya, D.; Bendahou, M.; Wink, J. Taxonomic Characterization, Antiviral Activity and Induction of Three New Kenalactams in *Nocardiostrictus* sp. CG3. *Curr. Microbiol.* **2022**, *79*, 284. [[CrossRef](#)]
75. The European Committee on Antimicrobial Susceptibility Testing (EUCAST). *Breakpoint Tables for Interpretation of MICs and Zone Diameters*; Version 10.0; European Committee on Antimicrobial Susceptibility Testing: Växjö, Sweden, 2020.
76. Benbelkhir, F.Z.; Benabdallah, N.; Messaoudi, O. Isolation and morphological characterization of myxobacteria from Algerian soil. In *Current Algerian Research Topics in Microbiology*; Sarahmed: Bejaia, Algeria, 2022; pp. 60–66.
77. CLSI. *Performance Standards for Antimicrobial Susceptibility Tests CLSI Standard M02*, 13th ed.; Clinical and Laboratory Standards Institute: Wayne, PA, USA, 2018.
78. Bellifa, S. Evaluation de la Formation du Biofilm des Souches de *Klebsiella pneumoniae* Isolées de Dispositifs Médicaux au CHU Tlemcen. Ph.D. Thesis, University of Tlemcen, Tlemcen, Algeria, 2014.
79. O'Toole, G.A. Microtiter Dish Biofilm Formation Assay. *J. Vis. Exp.* **2011**, *47*, e2437. [[CrossRef](#)]

Disclaimer/Publisher's Note: The statements, opinions and data contained in all publications are solely those of the individual author(s) and contributor(s) and not of MDPI and/or the editor(s). MDPI and/or the editor(s) disclaim responsibility for any injury to people or property resulting from any ideas, methods, instructions or products referred to in the content.